

Journal of Materials Chemistry A

Accepted Manuscript



This is an *Accepted Manuscript*, which has been through the Royal Society of Chemistry peer review process and has been accepted for publication.

Accepted Manuscripts are published online shortly after acceptance, before technical editing, formatting and proof reading. Using this free service, authors can make their results available to the community, in citable form, before we publish the edited article. We will replace this *Accepted Manuscript* with the edited and formatted *Advance Article* as soon as it is available.

You can find more information about *Accepted Manuscripts* in the [Information for Authors](#).

Please note that technical editing may introduce minor changes to the text and/or graphics, which may alter content. The journal's standard [Terms & Conditions](#) and the [Ethical guidelines](#) still apply. In no event shall the Royal Society of Chemistry be held responsible for any errors or omissions in this *Accepted Manuscript* or any consequences arising from the use of any information it contains.



www.rsc.org/materialsA

COMMUNICATION

Heteroatom-doped hierarchical porous carbons as high-performance metal-free oxygen reduction electrocatalysts†

Cite this: DOI: 10.1039/x0xx00000x

Received 00th January 2012,
Accepted 00th January 2012Yun-Pei Zhu,^a Youlin Liu,^a Yu-Ping Liu,^a Tie-Zhen Ren,^b Gao-Hui Du,^c Tiehong Chen^a and Zhong-Yong Yuan^{*a}

DOI: 10.1039/x0xx00000x

www.rsc.org/

Heteroatom-doped porous carbons with controllable dopant species were rationally synthesized through a universal polymerization-carbonization strategy, exhibiting considerable activity, superior resistance to methanol, and strong durability towards oxygen reduction in comparison with Pt/C benchmark, due to the doping effect and unique structural properties.

Exploiting highly active and cost-effective electrocatalysts for oxygen reduction reaction (ORR) is of paramount significance due to the indispensable role for researching fuel cells and metal-air batteries.¹ The inherently sluggish ORR kinetics requires exclusive utilization of noble metals, such as Pt, so as to achieve considerable activities,² whereas the unavoidable disadvantages are high cost, susceptibility to time-dependent potential drift, and easy deactivation by methanol poisoning and crossover effect. In this regard, the pursuit of alternative advanced electrocatalysts turns into a vital challenge. Accordingly, great efforts have been devoted to searching for substitutes through the use of nonprecious metal-based catalysts³ and even metal-free carbonaceous materials.⁴ Nonetheless, nonprecious metal-based catalysts usually suffer from the drawbacks of complicated fabrication, low conductivity, and detrimental environmental effects caused by catalyst residues. Distinctively, carbons have been emerging as promising ORR catalysts because of the essential peculiarities of tunable surface properties, sufficient electron conductivity, and outstanding corrosion resistance.

Further modification of carbons through foreign heteroatoms paves a way for tailoring the electron-donor properties and controlling the electronic and chemical states of the surface, thus enhancing the O₂ adsorption and reduction processes.⁵ Earth-abundant non-metal elements (N, P, S, B, etc.) have been successfully incorporated into carbonaceous frameworks via post-treatment and carbonization of heteroatom-enriched materials or composites of reactive heteroatom-containing

reagents and carbon precursors.⁶ Although great progress has been achieved in synthesizing heteroatom-modified carbons, the intentional tuning of dopant species remains challenging, and the serious inhibition of the practical applications lies in the expensive instruments and relatively harsh and time-consuming synthesis procedures. At this juncture, exploring new protocols to engineer heteroatom-doped carbons with fine structures and thereby favourable catalytic properties has received utmost attention.

In principle, introduction of abundant porosity into catalysts with high surface area and exposed catalytic sites as many as possible represents a persistent strategy to improve the electrocatalytic properties, due to the sufficient electroactive surface area, sophisticated pore channels to facilitate the mass transport, and multidimensional electron delivery pathways.⁷ Classical nanocasting, soft templating, and physical/chemical activation have been proven to be efficient to prepare porous carbonaceous materials,^{5a,8} though the bottlenecks of typical syntheses are complication and involvement of toxic substrates. In order to take advantage of the superiorities of carbons in practice, it is highly desirable to develop a facile methodology to synthesize porous carbocatalysts for high-performance ORR catalysis.

Herein, we propose a simple and novel one-step approach that involves the pyrolysis of organic acid and amine types induced precursors to prepare heteroatom-doped hierarchical meso-/macroporous carbon without using any templates and surfactants. This is capable of allowing the processes of carbonization and introduction of heteroatoms into the carbon frameworks, in which amine species and organic acids perform as heteroatom sources. Release of pyrolysis gas and reductive species can contribute to improve porosity and graphitization, which result in remarkable capacity to catalyze oxygen reduction with outstanding efficiency as compared with Pt/C benchmark but with better stability and methanol tolerance capability.

For the synthesis of hierarchical porous heteroatom-doped carbons, we first associate 1-hydroxyethylidene-1,1-diphosphonic acid (HEDP) with melamine to prepare N and P co-doped hierarchical porous carbons (NP-HPC) (for synthesis details, see ESI†). After the intimate mixing of HEDP and melamine, XRD patterns show appearance of a series of new diffractions and disappearance of diffractions related to HEDP and melamine (Fig. S1), and the characteristic bands corresponding to phosphonic and amine groups in the FT-IR spectra weaken and even disappear (Fig. S2), both of which reveal the generation of polymer analogues through the interaction between acid and base moieties. Thermostability analysis (Fig. S3) show that melamine completely sublimate at a temperature around 300 °C and HEDP is stable up to about 600 °C, while the stability of the resulting polymer analogous is elevated to a large extent, about 900 °C, and the sublimation can be significantly inhibited, which may be due to that HEDP possess a capacity to effectively link the melamine molecules.¹⁰

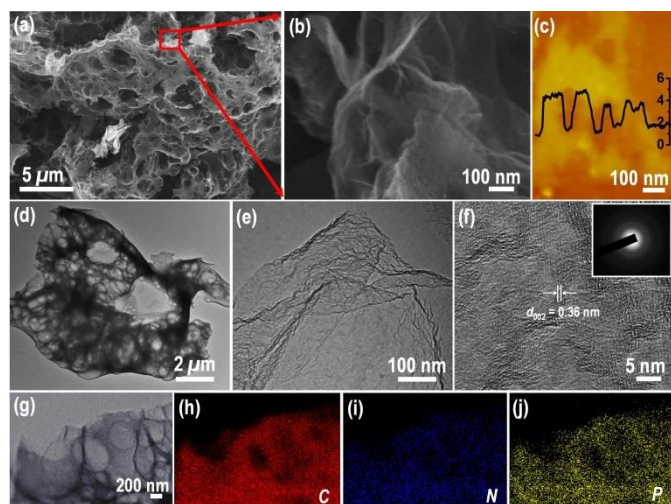


Fig. 1 (a,b) SEM, (c) AFM, and (d-f) TEM images of NP-HPC. Inset of (f) shows the SEAD pattern. (h-j) EDS elemental mapping images of NP-HPC.

The micromorphology and microstructures of the synthesized NP-HPC are illustrated by SEM and TEM. Low-magnification SEM and TEM images in Fig. 1a and 1d show foam-like structures, leaving randomly opened macropores of hundreds nanometers to several micrometers. Besides, the nearly transparent sheets signify the very thin thickness (Fig. 1b and 1e), coinciding with the atomic force microscopy (AFM) observations, which shows a thickness of 3-4.5 nm (Fig. 1c). High-magnification TEM image (Fig. 1f) indicates that NP-HPC is mainly consisted of graphitic layers, consistent with the selected area electron diffraction (SEAD) pattern. Energy dispersive X-ray spectroscopy (EDS) elemental mapping images of C, N, and P (Fig. 1h-j) verify that heteroatoms are effectively incorporated and homogeneously distributed throughout NP-HPC at the nanoscale.

XPS measurements are carried out to further probe the chemical state and stoichiometry. The C 1s spectra in Fig. S4 can be resolved into three components at 284.5 eV (sp^2 -

hybridized graphitic C), 285.9 eV ($N-sp^2$ C), and 287.8 eV ($N-sp^3$ C).^{10a} Analysis of N 1s spectra reveals the presence of pyridinic N, quaternary N, and pyridinic-N-oxides, ascribing to binding energies of 398.7, 401.1, and 404.5 eV, respectively (Fig. 2a).^{10b} These nitrogen functional groups are indicative of carbons that contain N atoms inserted into the carbonaceous backbone. Pyridinic N consists of nitrogen atoms doped at the edges of a graphitic carbon layer and graphitic N atoms are determined as quaternary N that is within a graphitic plane and bonded to three carbon atoms. As to the high-resolution P 2p region spectra (Fig. 2b), the dominant contribution located at 133.4 eV can be assigned to phosphate-like structures bound to carbon lattices,^{11a} while a weak peak situated at 135.1 eV is attributed to phosphate oxides.^{11b} There are 3.23 at% N and 2.57 at% P in NP-HPC depending on the XPS analysis.

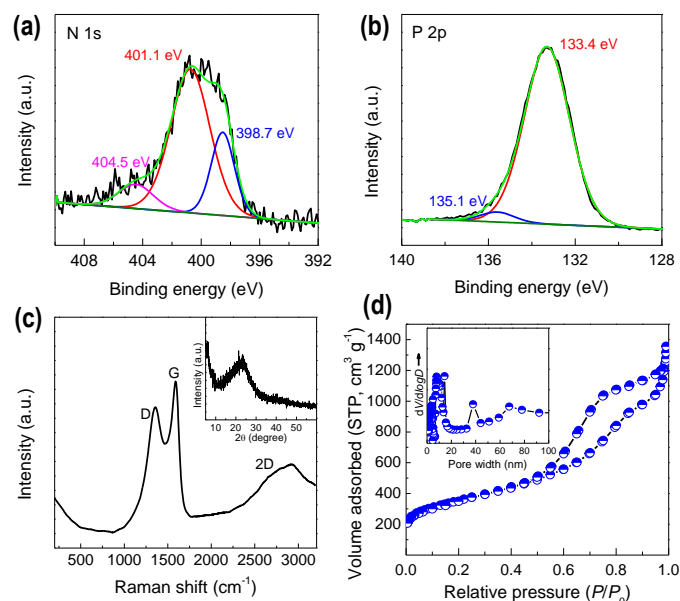


Fig. 2 (a,b) High-resolution XPS spectra of N 1s and P 2p in NP-HPC. (c) Raman spectra of NP-HPC, inset shows the wide-angle XRD pattern. (d) N_2 adsorption-desorption isotherm at 77 K with the corresponding pore size distribution (inset).

Raman spectroscopy in Fig. 2c shows two prominent peaks in the Raman spectrum at low frequency of 1378 cm^{-1} (D band) and 1582 cm^{-1} (G band) are attributable to imperfections in sp^2 carbon structures and the E_{2g} vibrational mode of sp^2 bonded carbon atoms in graphene sheets, respectively.¹² The broad 2D bands around 2700 cm^{-1} are characteristics of graphitic carbon materials.¹² The graphitic nature is further confirmed by the XRD pattern, which demonstrates a broad peak at approximately $2\theta = 24.2^\circ$, characteristics of the carbon (002) peak that is typical of graphitic carbon materials with a low degree of graphitization.¹³ Furthermore, the downshift of G band relative to pristine graphitic carbons provides evidence for the defective structures resulted from heteroatom doping effect.¹²

N_2 adsorption-desorption measurements are conducted to provide additional insights into the textural properties (Fig. 2d). The sorption isotherms are of characteristic type IV with distinct hysteresis loops of H2-type, suggesting the presence of large

amounts of mesopores, which is consistent with pore size distribution curve according to BJH model. The nitrogen volumes adsorbed rising steeply at high relative pressure (P/P_0) imply an appreciable amount of secondary porosity of large pores in the frameworks. These pores may be originated from the pyrolysis and gas escape during the high-temperature carbonization process. BET specific surface area and pore volume are determined to be $1283 \text{ m}^2 \text{ g}^{-1}$ and $1.72 \text{ cm}^3 \text{ g}^{-1}$, respectively.

Indeed, the acid-base derived precursors undergo thermal depolymerization, removal of volatiles, condensation, and aromatization during carbonization (Fig. S5). On one hand, the decomposition of base units can effectively reduce carbon matrixes^{14a} while produce N-containing species (e.g., C_2N_2^+ , C_3N_2^+ , C_3N_3^+)^{14b} that act as N sources for doping; on the other hand, phosphorus functionalities can react with the carbonaceous backbones at high temperature to form phosphate and phosphate oxide species.^{14c} Interestingly, a yellow-red solid deposited on the furnace walls, which comes from the thermal reduction of phosphorus functionalities by the carbonaceous residues,^{14d} is confirmed to be elemental phosphorus (Fig. S6). As a consequence, the favorable features of well-developed porosity, doping, and graphitization can contribute to boosting oxygen reduction.

Cyclic voltammetry (CV) measurements are performed on the heteroatom-doped porous carbons and referenced Pt/C to evaluate the catalytic activity towards ORR. As depicted in Fig. 3a, no obvious response can be observed in N_2 -saturated electrolyte, but a characteristic cathodic peak located at 0.822 V in O_2 environment in the same potential range. Noticeably, the ORR peak for Pt/C situates at 0.842 V (Fig. S7), only about 20 mV more positive in comparison with NP-HPC, revealing the electrochemical reduction of oxygen initiated on NP-HPC approach that of Pt/C. Also, similar tendency presents in linear sweep voltammetry (LSV) tests using a rotating disk electrode (RDE) (Fig. 3b). The NC-HPC catalyst displays almost equal ORR activity to that commercial Pt/C in terms of onset potential (0.949 V for NP-HPC and 0.952 V for Pt/C) and limiting current density (J_L , 4.98 mA cm^{-2} for NP-HPC and 4.86 mA cm^{-2} for Pt/C). Note that NC-HPC outperforms the state-of-the-art modified carbon-based electrocatalysts, and a detailed comparison is listed in Table S1. In contrast, the inferior activity for the materials synthesized from calcining at $800 \text{ }^\circ\text{C}$ for 2h and $900 \text{ }^\circ\text{C}$ for 5h can be due to that the incomplete pyrolysis at low temperature leads to lower surface area and increased stacking degree and loss of heteroatoms can occur after extending the calcination duration (Fig. S8).

Tafel curves are further employed to assess the structural superiorities of NP-HPC (Fig. 3c). The Tafel slopes of NP-HPC are fitted to be 85 mV dec^{-1} in the low overpotential range and 209 mV dec^{-1} in the high overpotential region, which are comparable to the Pt/C counterpart, revealing the superior reaction kinetics of NP-HPC. Such results indicate that the hierarchical porous peculiarity is beneficial to ensure the efficient mass transport across the pores and exposure of ORR active sites. A series of more detailed investigation of the RDE systems at various rotating speeds is taken to shed light on the ORR kinetics (Fig. S9). The current densities increase with the increase of rotating speed owing to the shortened diffusion distance at high speeds. The kinetic parameters including electron transfer number (n) and kinetic current density (J_k) are obtained according to Koutecky-Levich (K-L) equations (Fig. 3d and 3e). The good linearity of the K-L plots exhibits a first-order reaction with respect to the concentration of dissolved O_2 .¹⁵ From the slope of K-L plots, the n value per O_2 in the ORR process is 3.89 for NC-HPC, meaning the perfect selectivity (97.3%) for the pseudo-four-electron dominated ORR pathway. Moreover, NP-HPC possesses a higher J_k value of 23.8 mA cm^{-2} than that of Pt/C catalyst (20.2 mA cm^{-2}).

Recent experimental and theoretical studies in ORR reveal that the doping effect of N atoms in carbon backbones could introduce a defect in the nearby sited because of difference in bond length and atomic size and thus disrupt the electroneutrality of adjacent C atoms and create positively charged sites, which are favorable for O_2 adsorption and reduction.^{5,6} P has the same electron number as N and usually show similar chemical properties, making it promising as dopant species for carbons. Codoping with two elements could create a unique electronic structure with a synergistic coupling effect between heteroatoms,^{5,6,16} causing high ORR catalytic activity. In addition,

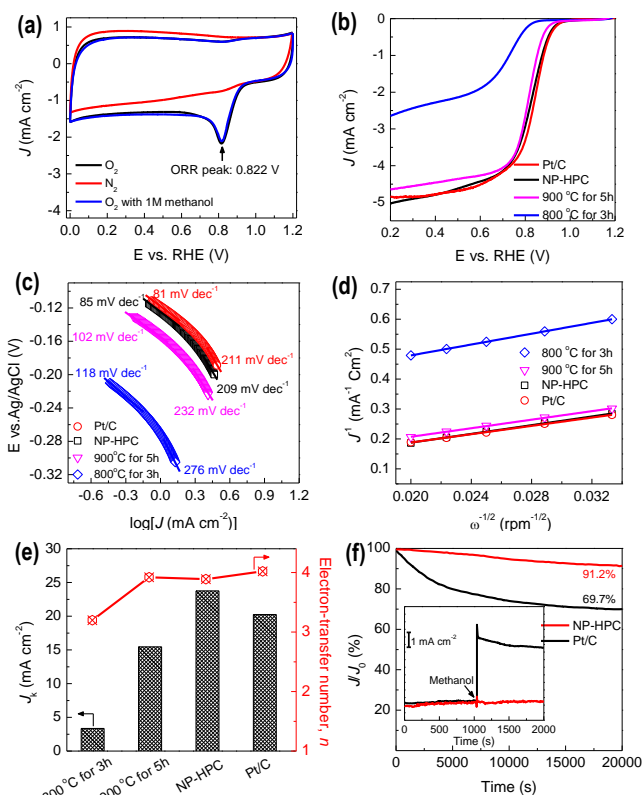


Fig. 3 (a) CV curves of NP-HPC in N_2 -saturated 0.1 M KOH , O_2 -saturated 0.1 M KOH , and O_2 -saturated 1 M methanol solutions, scan rate: 20 mV s^{-1} . (b) LSV and (c) Tafel curves of various materials in O_2 -saturated 0.1 M KOH at a scan rate of 10 mV s^{-1} at 1600 rpm . (d) K-L plots at 0.6 V . (e) Summary of the kinetic current density (J_k) and the electron-transfer number (n) on the basis of RDE data on various samples (at 0.6 V). (f) The chronoamperometric responses of NP-HPC and Pt/C at 0.7 V , inset: the chronoamperometric responses after adding methanol.

the spectacular porous architecture for NP-HPC is of great importance to offer cross-linked pore for electrolyte infiltration and high surface area for reaction and interfacial transport, and impressively, the graphitic nature endows the carbon network with precious electronic conductivity.

Besides high activity, NC-HPC shows a strong durability as measured by chronoamperometric response (Fig. 3f), with the ORR current density decreasing by 8.8% over 20000s of continuous operation under a constant cathodic voltage of 0.7 V, while Pt/C loses 30.3% of the initial current. Another crucial criterion for practical low temperature fuel cells is the high catalytic selectivity for cathode reactions against fuel oxidation. In the case of Pt/C, the cathodic current shifts to the anodic current immediately after adding methanol, which is accompanied by one new pair peak observed (Fig. S7), attributable to methanol oxidation-reduction, namely, a poisoning of catalyst. Distinctively, no activity specific to methanol is observed, and the characteristic ORR is maintained (Fig. 3a), indicating the high selectivity towards ORR (Fig. S10). These results imply that NP-HPC is a potential cathode catalyst for direct methanol fuel cells.

Interestingly, the organophosphonic acid could be reasonable substituted by other acid types to initiate the polymerization between acids and amines, such as sulfonic and carboxylic acids, and thus forming porous carbons with controllable doping species (Fig. S11). For instance, N,S co-doped hierarchical porous carbons, marked as NS-HPC, can be fabricated after the substitution phosphonic acids with sulfonic acids (Fig. S12). The coupling of carboxylic acid with bases can result in porous carbons of single N dopant (N-HPC, Fig. S13). It should be noted that heteroatom-doped porous carbons can be prepared in a broad combination of organic acids and bases (Fig. S14), confirming the feasibility and adaptability of the present acid-base polymerization-carbonization methodology. When we attempted to use the same route to synthesize modified carbon materials through utilizing inorganic acids (phosphoric, sulfuric, and carbonic acids), only inorganic salts could be obtained, which proved the functions of organic groups in bridging base units to form cross-linked polymer analogues. Both NS-HPC and N-HPC display high ORR activity, strong methanol tolerance and sufficient stability in alkaline media (Fig. S15 and S16).

In conclusion, we have disclosed a simple and universal strategy for the preparation of doped carbons and related composites by conjunction of suitable acid and base categories for the first time. These structures could exhibit considerable performance induced by the existence of porosity and heteroatoms, as herein described for electrochemical oxygen reduction application with excellent electrocatalytic activity, long-term stability, and resistance to alcohol crossover effect. This methodology not only holds promise to design functional carbon based materials, but also serves as a potential candidate for sustainable energy devices.

This work was supported by the National Natural Science Foundation of China (21421001), and the Natural Science Foundation of Tianjin (15JCZDJC37100).

Notes and references

^a Key Laboratory of Advanced Energy Materials Chemistry (Ministry of Education), Collaborative Innovation Center of Chemical Science and Engineering (Tianjin), College of Chemistry, Nankai University, 94 Weijin Road, Tianjin 300071, China. E-mail: zzyuan@nankai.edu.cn.

^b School of Chemical Engineering and Technology, Hebei University of Technology, Tianjin 300092, China.

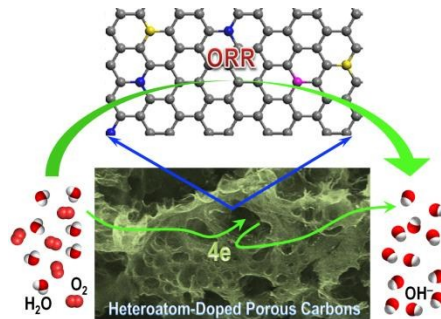
^c Institute of Physical Chemistry, Zhejiang Normal University, Jinhua 321004, China.

† Electronic Supplementary Information (ESI) available: Experimental procedures and detailed characterizations. See DOI: 10.1039/c000000x/

- (a) G. Wu, K. L. More, C. M. Johnston and P. Zelenay, *Science*, 2011, **332**, 443; (b) I. Katsounaros, S. Cherevko, A. R. Zeradjanin and K. J. J. Mayrhofer, *Angew. Chem., Int. Ed.*, 2014, **53**, 102.
- V. Mazumder, M. Chi, K. L. More and S. Sun, *J. Am. Chem. Soc.*, 2010, **132**, 7848.
- (a) Y. Hu, J. O. Jensen, W. Zhang, L. N. Cleemann, W. Xing, N. J. Bjerrum and Q. Li, *Angew. Chem., Int. Ed.*, 2014, **53**, 3675; (b) T. Y. Ma, S. Dai, M. Jaroniec and S. Z. Qiao, *J. Am. Chem. Soc.*, 2014, **136**, 13925.
- (a) Y. Zheng, Y. Jiao, J. Chen, J. Liu, J. Liang, A. Du, W. Zhang, Z. Zhu, S. C. Smith, M. Jaroniec, G. Q. Lu and S. Z. Qiao, *J. Am. Chem. Soc.*, 2011, **133**, 20116; (b) P. Zhang, F. Sun, Z. Xiang, Z. Shen, J. Yun and D. Cao, *Energy Environ. Sci.*, 2014, **7**, 442.
- (a) Y. Meng, D. Voiry, A. Goswami, X. Zou, X. Huang, M. Chhowalla, Z. Liu and T. Asefa, *J. Am. Chem. Soc.*, 2014, **136**, 13554; (b) W. He, C. Jiang, J. Wang and L. Lu, *Angew. Chem. Int. Ed.*, 2014, **53**, 9503; (c) R. Ning, J. Tian, A. M. Asiri, A. H. Qusti, A. O. Al-Youbi and X. Sun, *Langmuir*, 2013, **29**, 13146.
- (a) W. Wei, H. Liang, K. Parvez, X. Zhuang, X. Feng and K. Müllen, *Angew. Chem. Int. Ed.*, 2014, **53**, 1570; (b) H. L. Poh, P. Šimek, Z. Sofer and M. Pumera, *Chem.–Eur. J.*, 2013, **19**, 2655; (c) Y. J. Sa, C. Park, H. Y. Jeong, S. H. Park, Z. Lee, K. T. Kim, G. G. Park and S. H. Joo, *Angew. Chem., Int. Ed.*, 2014, **53**, 4102; (d) W. Yang, T. P. Fellinger and M. Antonietti, *J. Am. Chem. Soc.*, 2011, **133**, 206; (e) K. Gong, F. Du, Z. Xia, M. Durstock, L. Dai, *Science*, 2009, **323**, 760; (f) H. W. Liang, X. Zhuang, S. Brüller, X. Feng and K. Müllen, *Nat. Commun.*, 2014, **5**, 4973.
- S. H. Oh, R. Black, E. Pomerantseva, J. H. Lee, L. F. Nazar, *Nat. Chem.*, 2012, **4**, 1004.
- (a) Y. Zhu, S. Murali, M. D. Stoller, K. J. Ganesh, W. Cai, P. J. Ferreira, A. Pirkle and R. M. Wallace, K. A. Cychosz, M. Thommes, D. Su, E. A. Stach and R. S. Ruoff, *Science*, 2011, **332**, 1537; (b) T. Y. Ma, L. Liu and Z. Y. Yuan, *Chem. Soc. Rev.*, 2013, **42**, 3977.
- A. Thomas, A. Fischer, F. Goettmann, M. Antonietti, J. O. Müller, R. Schlögl, J. M. Carlsson, *J. Mater. Chem.* 2008, **18**, 4893.
- (a) A. L. M. Reddy, A. Srivastava, S. R. Gowda, H. Gullapalli, M. Dubey and P. M. Ajayan, *ACS Nano*, 2010, **4**, 6337; (b) Y. F. Lu, S. T. Lo, J. C. Lin, W. Zhang, J. Y. Lu, F. H. Liu, C. M. Tseng, Y. H. Lee, C. T. Liang and L. J. Li, *ACS Nano*, 2013, **7**, 6522.
- (a) M. Latorre-Sánchez, A. Primo and H. García, *Angew. Chem. Int. Ed.*, 2013, **52**, 11813; (b) J. M. Rosas, R. Ruiz-Rosas, J. Rodríguez-Mirasol and T. Cordero, *Carbon*, 2012, **50**, 1523.
- (a) K. N. Kudin, B. Ozbas, H. C. Schniepp, R. K. Prud'homme, I. A. Aksay and R. Car, *Nano Lett.*, 2008, **8**, 36; (b) B. Wang, X. L. Li, B.

- Luo, J. X. Yang, X. J. Wang, Q. Song, S. Y. Chen and L. J. Zhi, *Small*, 2013, **9**, 2399.
- 13 F. Zheng, Y. Yang and Q. Chen, *Nat. Commun.*, 2014, **5**, 5261.
- 14 (a) Z. Wen, X. Wang, S. Mao, Z. Bo, H. Kim, S. Cui, G. Lu, X. Feng and J. Chen, *Adv. Mater.*, 2012, **24**, 5610; (b) Z. H. Sheng, L. Shao, J. J. Chen, W. J. Bao, F. B. Wang and X. H. Xia, *ACS Nano*, 2011, **5**, 4350; (c) Y. Jiao, Y. Zheng, M. Jaroniec and S. Z. Qiao, *J. Am. Chem. Soc.*, 2014, **136**, 4394; (d) A. M. Puziy, O. I. Poddubnaya, A. Martínez-Alonso, F. Suárez-García and J. M. D. Tascón, *Carbon*, 2005, **43**, 2857.
- 15 Y. Liang, Y. Li, H. Wang, J. Zhou, J. Wang, T. Regier and H. Dai, *Nat. Mater.*, 2011, **10**, 780.
- 16 (a) H. Jiang, Y. Zhu, Q. Feng, Y. Su, X. Yang and C. Li, *Chem.–Eur. J.*, 2014, **20**, 3106; (b) Q. Li, R. Cao, J. Cho and G. Wu, *Adv. Energy Mater.*, 2014, **4**, 1301415; (c) D. Yu, Y. Xue and L. Dai, *J. Phys. Chem. Lett.*, 2012, **3**, 2863.

Table of Contents



Heteroatom-doped porous carbons synthesized through a universal polymerization-carbonization protocol exhibit considerable high activity and stability towards electrochemical oxygen reduction.